Afterslip and viscoelastic relaxation following the 2011 Tohoku-oki earthquake (M_w9.0) inferred from inland GPS and seafloor GPS/Acoustic data

Shuji Yamagiwa[1], Shin'ichi Miyazaki[1], Kazuro Hirahara[1], and Yukitoshi Fukahata[2]

[1]Graduate School of Science, Kyoto University, Kyoto, Japan, [2]Disaster Prevention Research Institute, Kyoto University, Uji, Kyoto, Japan

Abstract We simultaneously estimate 2.5 years of afterslip and viscoelastic relaxation, as well as coseismic slip, for the 2011 Tohoku-oki earthquake. Displacements at inland GPS and seafloor GPS/Acoustic stations are inverted using viscoelastic Green's functions for a model with an upper elastic layer and lower viscoelastic substrate. The result shows that afterslip is isolated from the rupture area and possibly asperities of historical earthquakes and has almost decayed by 10 September 2013, 2.5 years after the main shock. The inversion result also suggests that observed landward postseismic displacements at the seafloor GPS/Acoustic stations are caused by the viscoelastic relaxation, whereas trenchward displacements at inland stations are mainly an elastic response to afterslip.

1. Introduction

The 2011 Tohoku-oki earthquake (M_w9.0; 11 March 2011, at 5:46 UTC) is a giant earthquake at the Japan Trench, where the Pacific Plate subducts beneath northeast Japan in a direction nearly perpendicular to the trench at 9 cm/yr (Figure 1). This event was recorded by dense measurement arrays, such as the Japanese Global Navigation Satellite Systems Earth Observation Network, GEONET [e.g., *Ozawa et al.*, 2011]. The epicenter, 38.11°E, 142.92°N, is about 100 km away from the Pacific coast of Japan, making it difficult to resolve the slip distribution, only with GEONET. Recent improvements to seafloor geodetic measurements enabled us to investigate crustal deformation in offshore areas above the seismogenic zones [*Fujimoto*, 2014]. Coseismic and postseismic displacements have been recorded at seafloor GPS/Acoustic, or hereafter GPS/A, stations (Figure 1) [*Fujimoto*, 2014]. Coseismic slip distributions were better constrained by incorporating GPS/A data into inversion analyses [e.g., *Iinuma et al.*, 2012].

Directions of postseismic displacements for 2.5 years are found to be landward at GPS/A stations above the rupture region and to be trenchward at the rest of GPS/A stations and GEONET stations in the Tohoku district (Figure 2). For large earthquakes, three different mechanisms have been proposed to model postseismic deformation: afterslip [e.g., *Miyazaki et al.*, 2004], viscoelastic relaxation [e.g., *Diao et al.*, 2013], and poroelastic rebound [e.g., *Jónsson et al.*, 2003]. Among them, the duration of poroelastic rebound may be as short as a few weeks [e.g., *Peltzer et al.*, 1998]. Thus, this mechanism may not be appropriate to model the 2.5 years of postseismic deformation. The direction of afterslip is essentially similar to coseismic slip, because the shear stress increase due to coseismic slip triggers the afterslip. However, normal slip would be inferred if landward postseismic displacements were attributed to afterslip (Figure S1 in the supporting information). *Wang et al.* [2012] suggested that viscoelastic relaxation causes landward deformation above the oceanic mantle and trenchward above the mantle wedge. This suggests that it is difficult to distinguish afterslip and viscoelastic relaxation only from the data on land but, at the same time, implies the possibility to separate them if seafloor data are included.

The effect of viscoelastic relaxation has been considered on modeling postseismic deformation at subduction zones (e.g., *Hu et al.* [2004] for Chile, *Wang et al.* [2001] for Cascadia, and *Gunawan et al.* [2014] for Sumatra). Although the viscosity of the asthenosphere has not been well determined yet, most of the studies at subduction zones based on geodetic data obtained values of $0.5 - 5 \times 10^{19}$ Pa·s (see Table 1 of *Wang* [2007]). Independent of geodetic studies, *Rydelek and Sacks* [1988] obtained 7×10^{18} Pa·s in northeast Japan by investigating correlations between interplate and intraplate earthquakes there. On the other hand, analyses
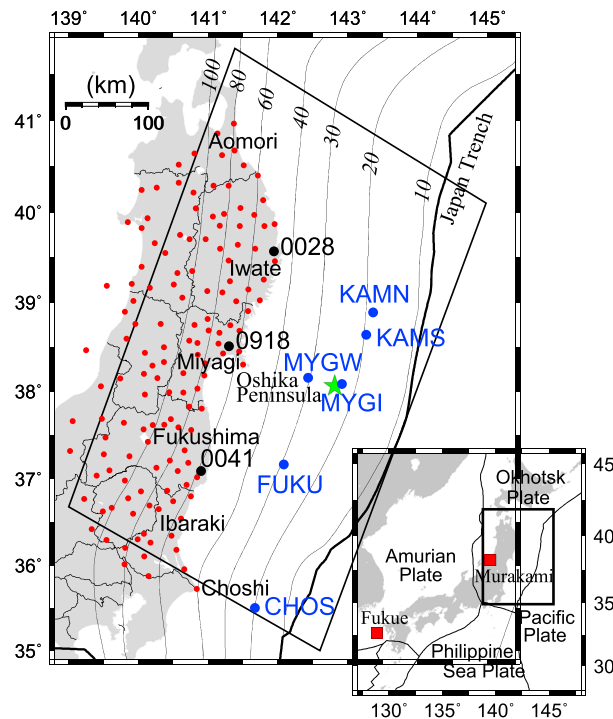
Figure 1. Configuration of the plate boundary and locations of observation stations. The inset shows the tectonic setting in and around Japan. The Pacific Plate is subducting westward beneath the Okhotsk Plate. The contours indicate the depth of the plate interface, and the numbers show the depths of the plate boundary [*Nakajima and Hasegawa*, 2006]. The modeled region of the plate boundary for the inversion analysis is indicated by the rectangle. The red and blue circles indicate the locations of the GEONET and seafloor GPS/A stations, respectively. The black circles show selected GEONET stations used in Figure S4 in the supporting information. The green star indicates the epicenter of the main shock on 11 March 2011. Red quadrangles in the inset show GEONET stations used as reference stations.

of loading data on the continental crust generally prefer viscosity of 10^{21}–10^{22} Pa·s [e.g., *Bills et al.*, 1994]. *Wang* [2007] pointed out that the relatively low viscosity at subduction zones may be related to additional fluids drained from the slab.

Diao et al. [2013] investigated postseismic deformation following the 2011 Tohoku-oki earthquake using the first 1.5 years of GEONET data and demonstrated that a combined model of afterslip and viscoelastic relaxation in an elastic-Maxwell viscoelastic media was preferable to a pure afterslip model. They suggested that the preferable values of the elastic thickness and viscosity were about 50 km and 2×10^{19} Pa·s, respectively, and that afterslip was dominant in the deeper extension of the rupture zone. However, their result may suffer from a lack of seafloor data, which have the potential to increase the resolution.

Here we study the postseismic deformation following the Tohoku-oki earthquake. We employ a horizontally layered elastic-viscoelastic medium and invert 2.5 years of data obtained at GEONET and seafloor GPS/A stations to infer coseismic slip, afterslip, and viscoelastic relaxation simultaneously.

2. Data

We use GPS/A data obtained by the Japan Coast Guard [*Watanabe et al.*, 2013], as well as daily GEONET data. To effectively solve the inverse problem, all GPS/A data are interpolated at the same epochs by fitting a piecewise linear function to each time series. The GEONET data are also resampled to obtain positions at the same epoch as the GPS/A data. Coseismic displacements at GPS/A stations are obtained by extrapolating station velocities between 30 March 2011 (the first postseismic GPS/A observation) and 1 May 2011 (the second postseismic observation) to 11 March 2011. We use displacements at six GPS/A and GEONET stations from 30 March 2011 ($t = 0.05$ year) to 10 September 2013 ($t = 2.50$ years) (i.e., for 2.45 years) as postseismic data, where $t = 0$ refers to the time of the main shock. All time series are then converted to displacements from $t = 0$ and then referenced to the position of Fukue station (Figure 1 for the location), where coseismic deformation is small and postseismic deformation is negligible. Finally, we subtract the predetermined secular velocity of Murakami station (Figure 1 for the location) relative to Fukue station to obtain displacements relative to Murakami. The obtained displacements are reasonable approximations to those relative to the Okhotsk Plate. Both the cumulative displacement (Figure 2) and time series data (Figure S4 in the supporting information) at the GEONET stations show trenchward postseismic deformation. In contrast, two GPS/A stations above the hypocentral region show landward postseismic movements, i.e., opposite to the direction expected from the afterslip alone (Figure 2 and Figure S4 in the supporting information).

3. Method of Inversion Analysis

We employ a model composed of an upper elastic layer overlying a homogeneous Maxwell viscoelastic substrate: the upper elastic layer represents the lithosphere, while the lower viscoelastic substrate represents the asthenosphere. Rigidity is set at 30 GPa in the elastic surface layer and 60 GPa in the viscoelastic substratum.
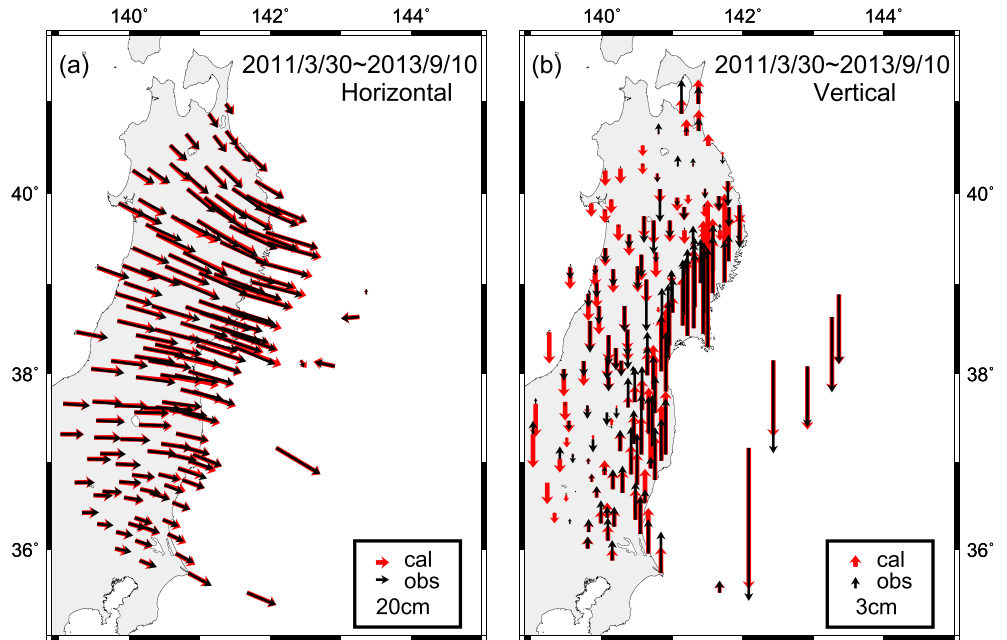
Figure 2. Comparison of observed (black arrows) and calculated (red arrows) postseismic deformation during the period from 30 March 2011 to 10 September 2013: (a) horizontal and (b) vertical components. The calculated deformation includes the viscoelastic relaxation due to the coseismic slip and the viscoelastic response due to afterslip.

The elastic thickness is set at 50 km following *Diao et al.* [2013]. The viscosity of the Maxwell body is set at 9.0×10^{18} Pa·s following *Suito and Hirahara* [1999] as a consistent value determined from previous studies at subduction zones. We employ the Pacific Plate configuration given by *Nakajima and Hasegawa* [2006], take a 400 km long and 300 km wide area as the model region (Figure 1) and divide it into 17×12 subfaults. We hereafter refer this region to the "model fault." Note that the Philippine Sea Plate is not included in our model. Thus, we will not study results for latitudes below 36°N.

Coseismic and postseismic displacements are represented by the sum of the following four components: elastic response to coseismic slip, elastic response to afterslip, viscoelastic relaxation caused by coseismic slip, and viscoelastic relaxation caused by afterslip. We employ an analytic expression of the Green's function for a viscoelastic response [*Fukahata and Matsu'ura*, 2006]. By arranging all displacements at all stations in a vector form, the observation equation for the ith component of the data vector is expressed as

$$d_i(\boldsymbol{x}, t) = \int_{-\infty}^{t} \int_F G_{ij}(\boldsymbol{x} - \xi, t - \tau)\, \dot{s}_j(\xi, \tau)\, dF(\xi)\, d\tau + e_i(\boldsymbol{x}, t) \tag{1}$$

where the subscript j represents the zstrike ($j = 1$) and dip ($j = 2$) components, respectively, d_i is the surface displacement, $\dot{s}_j$ is a slip rate, G_{ij} is the Green's function, and e_i is the random measurement error. The surface integral is done over the model fault F. We discretize the model fault into $K \times L$ patches, where K and L are the numbers of spatial basis functions in the length and width direction on the model fault, respectively. Thus, the slip rate is expressed as

$$\dot{s}_j(\xi, \tau) = \sum_{k=1}^{K} \sum_{l=1}^{L} \sum_{m=1}^{M} a_{jklm} X_{kl}(\xi) T_m(\tau) \tag{2}$$

where $X_{kl}(\xi)$ and $T_m(\tau)$ are the spatial and temporal basis functions, and M is the number of temporal basis functions. Boxcar functions are used as both spatial and temporal basis functions, and a_{jklm} are their coefficients. Substituting equation (2) into equation (1), we obtain the discrete version of the observation equation;

$$d_i(x, t) = \sum_{j=1}^{2} \sum_{k=1}^{K} \sum_{l=1}^{L} \sum_{m=1}^{M} H_{ijklm}(x, t)\, a_{jklm} + e_i(x, t) \tag{3}$$

with

$$H_{ijklm}(x, t) = \int_{-\infty}^{t} \int_F G_{ij}(\boldsymbol{x} - \xi, t - \tau) X_{kl}(\xi) T_m(\tau)\, dF(\xi)\, d\tau \tag{4}$$

Here coefficients a_{jklm} are the unknown model parameters to be determined from the inversion analysis. We also impose the constraint that the roughness of the slip distribution should be small in both space and time [*Yabuki and Matsu'ura*, 1992]. The relative weight of data to roughness constraints is optimized by minimizing the Akaike's Bayesian Information Criteria [*Akaike*, 1980]. It should be noted that slip, or slip rate, at any epoch is estimated from all data over the studied period.

Relative weights of different types/components of data are an important issue in constructing an inverse solution. In this paper, we use three displacement components of GEONET and GPS/A data. Some studies gave heavier weights to the horizontal components than vertical components observed at GEONET stations with a ratio of 3:1 [e.g., *Ozawa et al.*, 2004] and 5:1 [e.g., *Ozawa et al.*, 2012], while other studies [e.g., *Miyazaki et al.*, 2011; *Iinuma et al.*, 2012] gave an equal weight. We set weights of all components of GEONET and GPS/A displacements to be equal for the following two reasons. First, GEONET stations are distributed only in land, and mean distance between the nearest stations is about 20 km. In this case the off-diagonal terms of the covariance matrix (i.e., correlation) among nearby stations should not be neglected [*Yagi and Fukahata*, 2011]. Inclusion of covariance among GEONET stations would effectively downweight GEONET data. Therefore, if the covariance among GEONET stations is neglected for simplicity, it should be offset by more weight on GPS/A stations. Second, as *Iinuma et al.* [2012] claims, model errors (i.e., errors caused by inaccuracies of Green's functions) are significantly larger than the measurement error especially in case of the 2011 Tohoku-oki earthquake. Model errors are often assumed to be proportional to the signal amplitude. Postseismic displacements are several tens of centimeters in horizontal and a few tens of centimeters in vertical, including GPS/A stations (Figure 2). Consequently, they are basically at the same order of magnitude for the horizontal and vertical components and would be comparable to or larger than measurement errors, which are about 3 mm in horizontal and 15 mm in vertical for GEONET [*Nakagawa*, 2009] and about 3 cm for GPS/A in northeast Japan [*Sato*, 2012; *Fujimoto*, 2014]. Therefore, it may be a reasonable approximation to set weights equally for all three components of both GEONET and GPS/A data.

The resolution of the inversion is investigated by a checkerboard test (Figure S2 in the supporting information). Slip areas larger than 90 km are resolved, except for most areas near the trench. However, even near the trench, 90 km of slip area could be resolved in some areas, e.g., for the area off Miyagi prefecture.

4. Results

4.1. Coseismic Slip

The inverted coseismic slip distribution is presented in Figure 3a. The maximum slip of about 50 m is found at depths shallower than 35 km. In addition, 10–20 m of slip is estimated in the areas of off-Iwate prefecture and off-Ibaraki prefecture. Note that coseismic slips associated with two thrust aftershocks at off-Iwate prefecture ($M_w = 7.4$, 11 March 2011 at 6:08 UTC) and off-Ibaraki prefecture ($M_w = 7.6$, 11 March 2011 at 6:15 UTC) are included in this coseismic slip. Thus, the estimated coseismic slip may be smeared over these regions. The estimated moment release is 4.65×10^{22} Nm, and the corresponding moment magnitude is 9.0. Our result is consistent with previous studies [e.g., *Ozawa et al.*, 2012; *Iinuma et al.*, 2012; *Diao et al.*, 2013] in the point that slip is concentrated near the trench. Some difference in spatial distribution may be attributed to the difference in the weighting of GEONET data, GPS/A data, the strength of spatial smoothness prior, and the consistency with viscoelastic relaxation.

4.2. Afterslip

Space-time evolution of afterslip is estimated for the period from 30 March 2011 to 10 September 2013 (Figure S3 in the supporting information). The cumulative afterslip distribution reveals two slip maxima on the plate boundary deeper than 40 km between 37°N and 40°N, as shown in Figure 3b. Similar afterslip distributions have been estimated by *Ozawa et al.* [2012], *Diao et al.* [2013], and *Silverii et al.* [2014] without GPS/A data. Two to three meters of afterslip was also estimated in a shallower part of the plate boundary in the off-Fukushima area. Despite of poor resolution, the maximum slip there of about 1.4 m is significantly beyond the confidence interval of about 0.6 m. As has been pointed out for other earthquakes, afterslip is inferred where coseismic slip was not estimated, probably because of the spatial variation of frictional properties [*Miyazaki et al.*, 2004]. Our inversion result shows that afterslip has almost decayed by 10
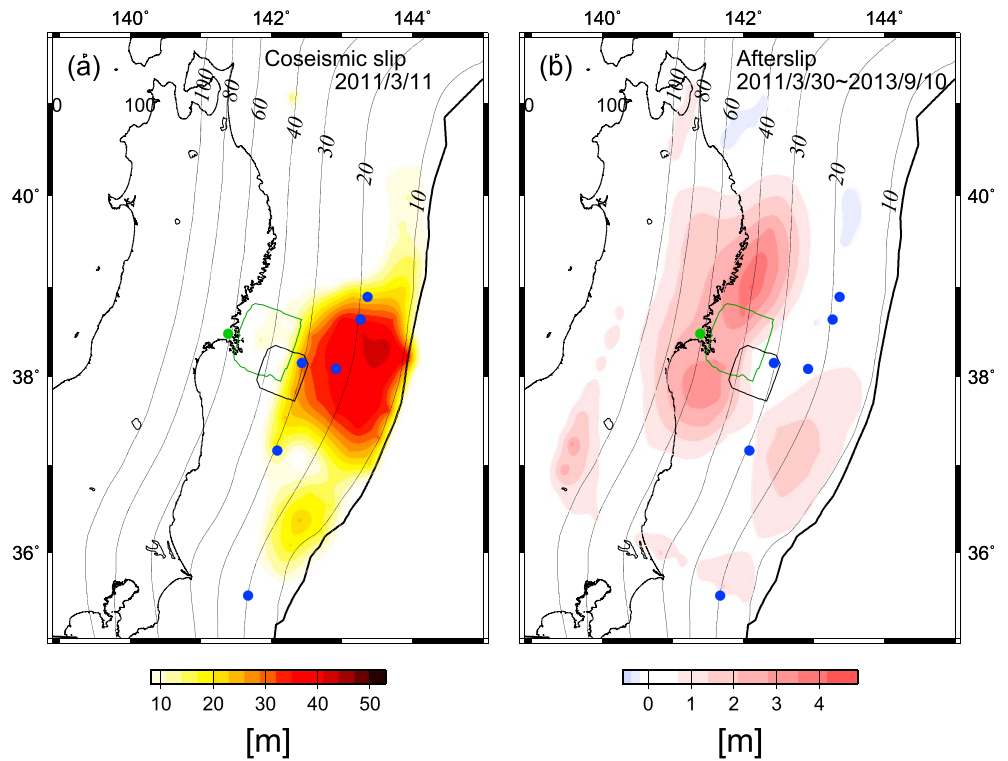
Figure 3. (a) Coseismic slip distribution on 11 March 2011 and (b) afterslip distribution over the period from 30 March 2011 to 10 September 2013. Zero slip in Figure 3b corresponds to the slip at the plate convergence rate of the Pacific Plate. The red contours denote the excess reverse fault slip, and the blue contours denote the slip deficit. The areas enclosed by the green and black lines in Figure 3b represent the 1978 Miyagi-oki and the 1936 Miyagi-oki asperities, respectively [*Yamanaka and Kikuchi*, 2004]. The green and blue circles show selected GEONET and GPS/A stations, respectively.
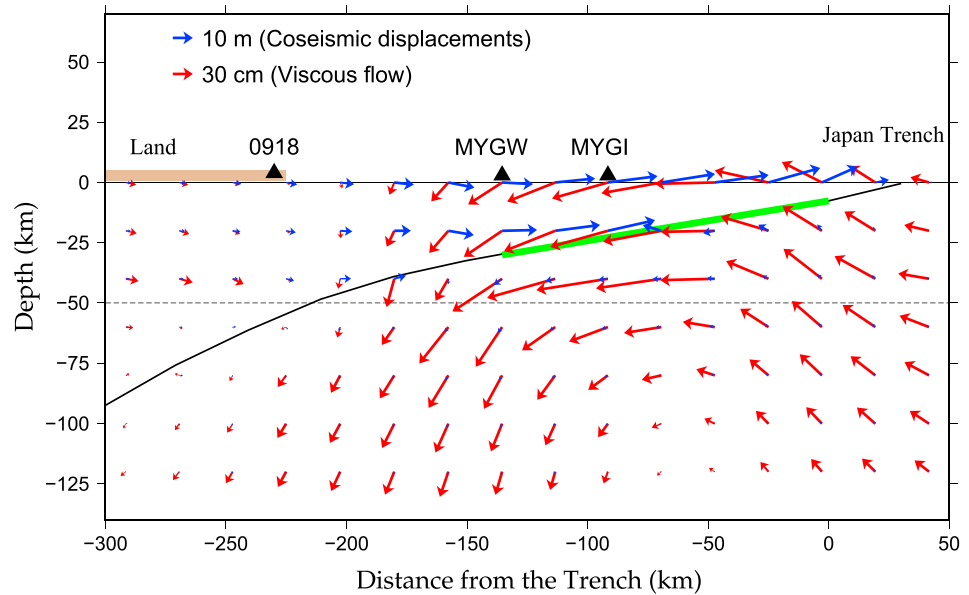

Figure 4. Coseismic displacements and cumulative displacements due to viscoelastic relaxation at depth projected onto the vertical section along the line connecting the three stations, 0918, MYGW, and MYGI (see Figure 1 for station locations.). The red arrows indicate the displacements due to viscoelastic relaxation induced by coseismic slip and afterslip over the period from 30 March 2011 to 10 September 2013. The blue arrows indicate the displacements due to coseismic slip. The black triangles indicate the observation stations. The brown line indicates the area of land. The solid black line indicates the plate boundary. The green line represents the part of the fault where the coseismic slip was over 30 m. The black broken line shows the boundary between elastic and viscoelastic layers.
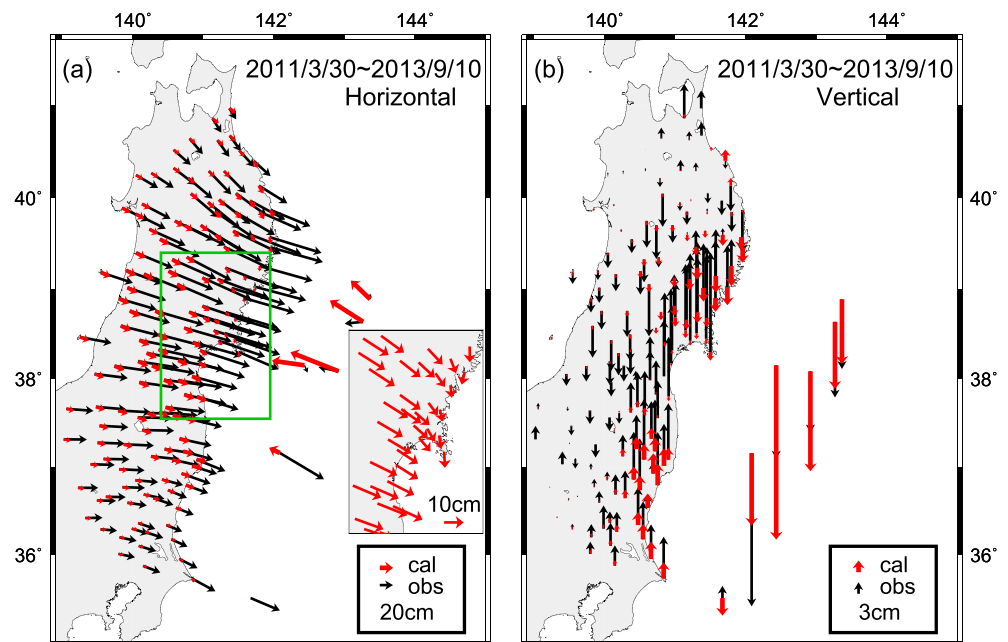
Figure 5. Comparison of observed postseismic displacements (black) and calculated displacements only due to viscoelastic relaxation (red): (a) horizontal and (b) vertical components. The inset in Figure 5a shows the magnified horizontal displacements due to viscoelastic relaxation of the area shown by the green rectangular. Displacements due to viscoelastic relaxation include both the effects of the coseismic slip and the afterslip estimated by the inversion analysis. Comparison of these diagrams with those in Figure 2 enables us to understand how the viscoelastic relaxation due to the coseismic slip and afterslip contributes to the postseismic deformation observed in seafloor and inland areas.

September 2013 (Figure S3 in the supporting information). The total moment release by afterslip is 9.94×10^{21} Nm during the studied period, which corresponds to $M_w = 8.6$.

4.3. Viscoelastic Relaxation due to Coseismic Slip and Afterslip

Time-dependent viscous flow driven by stress relaxation in the asthenosphere is obtained simultaneously in our inversion. A cross section of the viscous flow along the line connecting three stations, 0918, MYGW, and MYGI is shown in Figure 4 (See Figure 1 for station locations.). The cumulative displacements of the viscous flow at depths are characterized by a counterclockwise rotation in the area of -200 km $< L <$ 50 km, where L is the landward distance from the trench. We also see trenchward movements above the plate boundary in the area of $L <$ -200 km. The resultant surface displacements are shown in Figure 5. GPS/A stations are predicted to subside (e.g., 25 cm at MYGI and 42 cm at MYGW) and move landward (e.g., 70 cm at MYGI and 47 cm at MYGW) except for CHOS (Figure 5a). Similar viscoelastic displacements, i.e., subsidence and landward motion above the large slip area, have also been demonstrated by *Hashima et al*. [2014]. The viscoelastic relaxation also causes small subsidence (e.g., 2 cm at 0918) and trenchward movements (e.g., 4 cm at 0918) at inland stations above the downdip extension of the large coseismic slip area, while it causes uplift and trenchward movements at the rest of the inland stations (Figure 5b).

We compute surface displacements at observation stations due to the sum of the afterslip and viscoelastic relaxation. Fits to observed data (Figure 2 and Figure S4 in the supporting information) are reasonably good. The root-mean-square of the residuals is 3.56 cm (Figure S5 in the supporting information).

5. Discussion

In order to examine the effect of the relative weight of different kinds of observed data, we carried out two more cases of inversion analyses, in which the relative weight of the GEONET horizontal, GEONET vertical, and all three components of GPS/A are taken to be 12:4:1 and 20:4:1. Note that the latter is the same weight as that *Ozawa et al*. [2012] used. In both cases, uplift is predicted at MYGW and FUKU, where subsidence is observed. On the contrary, subsidence is predicted at CHOS, where uplift is observed. We have not examined whether heavier weighting of GPS/A over GEONET produces significant differences because the residuals of

GPS/A data are comparable to those of the GEONET data even in the case of the equal weight. Therefore, we consider it reasonable to equally weight all components of both the GEONET and GPS/A stations.

We have assumed that the asthenosphere is a Maxwell body and set the viscosity to 9.0×10^{18} Pa·s. The result of underestimating the viscoelastic contribution to the postseismic deformation is that normal sense afterslip is inferred to be similar to the fully elastic solution (Figure S1 in the supporting information). Since the inferred afterslip is more reasonable for what would be expected in subduction zones, the choice of viscosity $\sim 10^{19}$ Pa·s is reasonable.

Despite the spatial smoothing, dominant inferred afterslip including shallow slip in the off-Fukushima area seems to avoid asperities of historical earthquakes since 1896 (see Figure 1 of *Johnson et al.* [2012] for the asperity locations). For example, ~10 m of coseismic slip was inferred for the 1936 Miyagi-oki earthquake and the 1978 Miyagi-oki earthquake asperities (Figure 3a), and cumulative afterslip seems to avoid those locations. Thus, the inferred cumulative afterslip is consistent with the conventional asperity model, and hence, asperities of historical earthquakes may be loaded by the sustained afterslip. However, this should be carefully examined in a way such as proposed by *Johnson et al.* [2012].

Surface displacements caused by afterslip and viscoelastic relaxation resemble each other at the GEONET stations. This makes it difficult to distinguish these two postseismic processes only from inland GPS measurements (see inland area of Figure 4). While the predicted displacements due to viscoelastic relaxation are trenchward at inland GPS stations, they are landward, and almost parallel to the subduction direction of the Pacific Plate, at GPS/A stations above the hypocentral area. Based on the inversion analysis with GPS/A data using a simple elastic-viscoelastic layered model, it is inferred that the landward movements at GPS/A stations are essentially due to viscoelastic relaxation. Because the nominal relaxation time of the viscoelastic asthenosphere is 9.5 years, viscoelastic deformation will continue over one century. With the Green's functions we used, trenchward movements due to viscoelastic relaxation may reach up to about 1 m at the maximum on the Pacific coastal area of the Tohoku district over 100 years.

Our inversion results show that afterslip causes uplift of about 20–30 cm at inland stations above the downdip extension of the large slip area over the studied period, while viscoelastic relaxation causes subsidence of about a few centimeters there. Since the afterslip is almost over as of September 2013, subsidence would be expected there. In addition to the coseismic subsidence, interseismic deformation in this area was also subsidence of 1–10 mm/yr [*Nishimura*, 2012]. This conflicts with a geomorphological study that shows that the Pacific coastal area has been uplifted at a rate of 0.1 mm/yr [*Koike and Machida*, 2001]. Our preliminary investigation suggests that larger uplift tends to be predicted if we employ a thinner elastic layer. Thus, the employment of a more realistic Earth model [e.g., *Sun et al.*, 2014] may resolve this issue.

References

Akaike, H. (1980), Likelihood and the Bayes procedure, in *Bayesian Statistics*, edited by J. M. Bernardo et al., pp. 143–166, Univ. Press, Valencia.

Bills, G. B., D. R. Currey, and G. A. Marshall (1994), Viscosity estimates for the crust and upper mantle from patterns of lacustrine shoreline deformation in the eastern Great Basin, *J. Geophys. Res.*, *99*, 22,059–22,086, doi:10.1029/94JB01192.

Diao, F., X. Xiong, R. Wang, Y. Zheng, T. R. Walter, H. Weng, and J. Li (2013), Overlapping postseismic deformation processes: Afterslip and viscoelastic relaxation following the 2011Mw 9.0 Tohoku (Japan) earthquake, *Geophys. J. Int.*, *196*, 218–229, doi:10.1093/gji/ggt376.

Fujimoto, H. (2014), Seafloor geodetic approaches to subduction thrust earthquakes, *Monogr. Environ. Earth Planets*, *2*, 23–63, doi:10.5047/meep.2014.00202.0023.

Fukahata, Y., and M. Matsu'ura (2006), Quasi-static internal deformation due to a dislocation source in a multilayered elastic/viscoelastic half-space and an equivalence theorem, *Geophys. J. Int.*, *166*, 418–434, doi:10.1111/j.1365-246X.2006.02921.x.

Gunawan, E., T. Sagiya, T. Ito, F. Kimata, T. Tabei, Y. Ohta, I. Meilano, H. Z. Abidine, I. N. Agustan, and D. Sugiyanto (2014), A comprehensive model of postseismic deformation of the 2004 Sumatra-Andaman earthquake deduced from GPS observations in northern Sumatra, *J. Asian Earth Sci.*, *88*, 218–229, doi:10.1016/j.jseaes.2014.03.016.

Hashima, A., Y. Fukahata, C. Hashimoto, and M. Matsu'ura (2014), Quasi-static strain and stress fields due to a moment tensor in elastic-viscoelastic layered half-space, *Pure Appl. Geophys.*, doi:10.1007/s00024-013-0728-0.

Hu, Y., K. Wang, J. He, J. Klotz, and G. Khazaradze (2004), Three-dimensional viscoelastic finite element model for postseismic deformation of the great 1960 Chile earthquake, *J. Geophys. Res.*, *109*, B12403, doi:10.1029/2004JB003163.

Iinuma, T., et al. (2012), Coseismic slip distribution of the 2011 off the Pacific Coast of Tohoku Earthquake (M9.0) refined by means of seafloor geodetic data, *J. Geophys. Res.*, *117*, B07409, doi:10.1029/2012JB009186.

Jónsson, S., P. Segall, R. Pedersen, and G. Björnsson (2003), Postearthquake, ground movements correlated to pore-pressure transients, *Nature*, *424*, 179–183.

Johnson, K. M., J. Fukuda, and P. Segall (2012), Challenging the rate-state asperity model: Afterslip following the 2011 M9 Tohoku-oki, Japan, earthquake, *Geophys. Res. Lett.*, *39*, L20302, doi:10.1029/2012GL052901.

Koike, K., and H. Machida (2001), *Atlas of Quaternary Marine Terraces in Japanese Island* [in Japanese], 122 pp., Univ. Tokyo Press, Tokyo.

Miyazaki, S., P. Segall, J. Fukuda, and T. Kato (2004), Space time distribution of afterslip following the 2003 Tokachi-oki earthquake: Implications for variations in fault zone frictional properties, *Geophys. Res. Lett.*, *31*, L06623, doi:10.1029/2003GL019410.

Miyazaki, S., J. J. McGuire, and P. Segall (2011), Seismic and aseismic fault slip before and during the 2011 off the Pacific coast of Tohoku Earthquake, *Earth Planets Space*, *63*, 637–642.

Nakagawa, H. (2009), Development and validation of GEONET new analysis strategy (Version 4) [in Japanese], *J. Geogr. Surv. Inst.*, *118*, 1–8.

Nakajima, J., and A. Hasegawa (2006), Anomalous low-velocity zone and linear alignment of seismicity along it in the subducted Pacific slab beneath Kanto, Japan: Reactivation of subducted fracture zone?, *Geophys. Res. Lett.*, *33*, L16309, doi:10.1029/2006GL026773.

Nishimura, T. (2012), Crustal deformation of northeastern Japan based on geodetic data for recent 120 years [in Japanese with English abstract], *Geol. Soc. Jpn.*, *118*, 278–293.

Ozawa, S., M. Kaizu, M. Murakami, T. Imakiire, and Y. Hatanaka (2004), Coseismic and postseismic crustal deformation after the Mw 8 Tokachi-oki earthquake in Japan, *Earth Planets Space*, *56*, 675–680.

Ozawa, S., T. Nishimura, H. Suito, T. Kobayashi, M. Tobita, and T. Imakiire (2011), Coseismic and postseismic slip of the 2011 magnitude-9 Tohoku-oki earthquake, *Nature*, *475*, 373–376, doi:10.1038/nature10227.

Ozawa, S., T. Nishimura, H. Munekata, H. Suito, T. Kobayashi, M. Tobita, and T. Imakiire (2012), Preceding, coseismic, and postseismic slips of the 2011 Tohoku earthquake, Japan, *J. Geophys. Res.*, *117*, B07404, doi:10.1029/2011JB009120.

Peltzer, G., P. Rosen, F. Rogez, and K. Hudnut (1998), Poroelastic rebound along the Landers 1992 earthquake surface rupture, *J. Geophys. Res.*, *103*, 30,131–30,145, doi:10.1029/98JB02302.

Rydelek, P., and I. Sacks (1988), Asthenospheric viscosity inferred from correlated land–sea earthquakes in north-east Japan, *Nature*, *336*, 234–237, doi:10.1038/336234a.

Sato, M. (2012), Elucidation of seafloor crustal movements off northeastern Japan by GPS/acoustic technique with evaluation of sailing observation data from hull-mounted system, Doctor thesis, 93 p., Tohoku Univ., Sendai.

Silverii, F., D. Cheloni, N. D'Agostino, G. Selvaggi, and E. Boschi (2014), Post-seismic slip of the 2011 Tohoku-Oki earthquake from GPS observations: Implications for depth-dependent properties of subduction megathrusts, *Geophys. J. Int.*, *198*, 580–596, doi:10.1093/gji/ggu149.

Suito, H., and K. Hirahara (1999), Simulation of postseismic deformations caused by the 1896 Riku-u earthquake, northeast Japan: Re-evaluation of the viscosity in the upper mantle, *Geophys. Res. Lett.*, *26*, 2561–2564, doi:10.1029/1999GL900551.

Sun, T., et al. (2014), Prevalence of viscoelastic relaxation after the 2011 Tohoku-oki earthquake, *Nature*, *514*, 84–87, doi:10.1038/nature13778.

Wang, K. (2007), Elastic and viscoelastic models of subduction earthquake cycles, in *The Seismogenic Zone of Subduction Thrust Faults*, vol. 640, pp. 540–575, Columbia Univ. Press, New York.

Wang, K., J. He, H. Dragert, and T. James (2001), Three-dimensional viscoelastic interseismic deformation model for the Cascadia subduction zone, *Earth Planets Space*, *53*, 295–306.

Wang, K., Y. Hu, and J. He (2012), Deformation cycles of subduction earthquakes in a viscoelastic Earth, *Nature*, *484*, 327–332, doi:10.1038/nature11032.

Watanabe, S., M. Sato, T. Ishikawa, N. Ujihara, M. Mochizuki, and A. Asada (2013), Postseismic seafloor movements due to the 2011 Tohoku Earthquake detected by GPS/acoustic geodetic observation [in Japanese], *Abstr. of Seism. Soc. Jpn. 2013 Fall Meet.*

Wessel, P., and W. H. F. Smith (1998), New, improved version of the Generic Mapping Tools released, *Eos Trans. AGU*, *79*, 579, doi:10.1029/98EO00426.

Yabuki, T., and M. Matsu'ura (1992), Geodetic data inversion using a Bayesian information criterion for spatial distribution of fault slip, *Geophys. J. Int.*, *109*, 363–375.

Yagi, Y., and Y. Fukahata (2011), Introduction of uncertainty of Green's function into waveform inversion for seismic source processes, *Geophys. J. Int.*, *186*, 711–720.

Yamanaka, Y., and M. Kikuchi (2004), Asperity map along the subduction zone in northeastern Japan inferred from regional seismic data, *J. Geophys. Res.*, *109*, B07307, doi:10.1029/2003JB002683.